SCIENTIFIC REPORTS

OPEN

SUBJECT AREAS:
ELECTRONIC PROPERTIES AND MATERIALS
NANOPARTICLES
CATALYST SYNTHESIS
CARBON NANOTUBES AND FULLERENES

Received
9 November 2012

Accepted
25 February 2013

Published
15 March 2013

Correspondence and requests for materials should be addressed to M.S.H. (maoshuai.he@aalto.fi) or H.J. (hua.jiang@aalto.fi)

Chiral-Selective Growth of Single-Walled Carbon Nanotubes on Lattice-Mismatched Epitaxial Cobalt Nanoparticles

Maoshuai He[1], Hua Jiang[2], Bilu Liu[2,3], Pavel V. Fedotov[4], Alexander I. Chernov[4], Elena D. Obraztsova[4], Filippo Cavalca[5], Jakob B. Wagner[5], Thomas W. Hansen[5], Ilya V. Anoshkin[2], Ekaterina A. Obraztsova[4], Alexey V. Belkin[4], Emma Sairanen[1], Albert G. Nasibulin[2], Juha Lehtonen[1] & Esko I. Kauppinen[2]

[1]Department of Biotechnology and Chemical Technology, School of Chemical Technology, Aalto University, P.O. Box 16100, FI-00076 Aalto, Finland, [2]NanoMaterials Group, Department of Applied Physics and Center for New Materials, School of Science, Aalto University, P.O. Box 15100, FI-00076 Aalto, Finland, [3]Shenyang National Laboratory for Materials Science, Institute of Metal Research, Chinese Academy of Sciences, Shenyang 110016, P. R. China, [4]A.M. Prokhorov General Physics Institute RAS, 38 Vavilov Street, 119991 Moscow, Russia, [5]Center for Electron Nanoscopy, Technical University of Denmark, DK-2800 Kongens Lyngby, Denmark.

Controlling chirality in growth of single-walled carbon nanotubes (SWNTs) is important for exploiting their practical applications. For long it has been conceptually conceived that the structural control of SWNTs is potentially achievable by fabricating nanoparticle catalysts with proper structures on crystalline substrates via epitaxial growth techniques. Here, we have accomplished epitaxial formation of monometallic Co nanoparticles with well-defined crystal structure, and its use as a catalyst in the selective growth of SWNTs. Dynamics of Co nanoparticles formation and SWNT growth inside an atomic-resolution environmental transmission electron microscope at a low CO pressure was recorded. We achieved highly preferential growth of semiconducting SWNTs (~90%) with an exceptionally large population of (6, 5) tubes (53%) in an ambient CO atmosphere. Particularly, we also demonstrated high enrichment in (7, 6) and (9, 4) at a low growth temperature. These findings open new perspectives both for structural control of SWNTs and for elucidating the growth mechanisms.

An ultimate goal in the field of carbon nanotube research is to attain SWNTs with controlled chiralities[1,2]. Although significant progress has been made in chirality separation of SWNTs by a number of post-synthesis approaches[2], such as density gradient centrifugation[3,4], DNA wrapping chromatography[5–7], and multicolumn gel chromatography[8], direct selective growth of SWNTs with a narrow chirality distribution[9–17] is still regarded as an irreplaceable approach to achieve the goal without deteriorating the pristine structure and modifying the electronic properties of the SWNTs. Over the last decade, substantial efforts have been devoted to developing various structure-controlled synthesis methods[9–17], of which most are based on the catalytic chemical vapor deposition (CVD) method[9–16], known to be an economic and controllable process for carbon nanotube production. It has been discovered that, in the CVD process, SWNTs nucleate and grow on active catalytic nanoparticles and the size and crystal structure of those nanoparticles play a key role in determining the chiral structures of the produced SWNTs[18–20]. However, in most instances, metal nanoparticle catalysts have too broad distribution of size and microstructure due to the lack of efficient control on nanoparticle formation[21–23]. Furthermore, the orientations of energetic nanoparticles tend to fluctuate considerably[24,25], causing variability in the early stage of SWNT nucleation and growth[26]. Therefore, in order to achieve a high chiral selectivity in SWNT growth, one needs to seek an efficient way to have effective size and structure control of those catalytic nanoparticles.

Both theoretical[27] and experimental studies[28,29] have shown that metal nanoparticles epitaxially formed from the basal plane of the catalyst support usually exhibit a well-defined crystal structure and a uniform morphology. It has been conceptually conceived for long that the structural control of SWNTs is potentially achievable by using such epitaxial nanoparticle catalysts with proper structures for templated growth[25,30]. However, to the best of our

knowledge, no one has been able to grow SWNTs on such epitaxially-formed nanoparticles with the aim of enhancing their chiral selectivity.

MgO-based solid solutions as catalysts have been used to grow carbon nanotubes[31–33]. Due to the similarity in their structures, many transition metals oxides (e.g. CoO, NiO) are completely miscible with MgO and they can easily form ideal solid solutions[31–34]. In such solid solutions, the transition metal cations (Co^{2+} or Ni^{2+}) have strong interactions with MgO. Thus, by reduction of the solid solution, only a small portion of metal cations are expected to be reduced and form small nanoparticles on the surface[34]. The metal nanoparticles are usually well dispersed and stabilized by the MgO support, which favor carbon nanotube production[31–33]. However, due to a lack of control over the nanoparticle formation in earlier works, both the morphology and the crystal structure of those metal nanoparticles are varied, resulting in the production of either multi-walled carbon nanotubes[31,33] or SWNTs with a range of chiral species[32].

In this work, we have successfully accomplished an epitaxial formation of Co nanoparticles by the reduction of $Co_xMg_{1-x}O$ solid solution in CO, which was, for the first time, employed to grow SWNTs with a strong chiral preference. The $Co_xMg_{1-x}O$ solid solution was prepared under optimal calcination conditions so that, upon reduction, the Co precipitated at a low rate[35], leading to an epitaxial formation of Co nanoparticles on the surface of the MgO support. *In situ* environmental transmission electron microscopy (E-TEM) was employed to study the dynamics of catalytic Co nanoparticle evolution. Growth of SWNTs inside the microscope in the presence of CO at a low pressure was accomplished and examined in real time. The epitaxial relationship between the Co nanoparticles and the MgO matrix was investigated. Monodisperse Co nanoparticles were found to be anchored epitaxially to the MgO support and they exhibited little structural fluctuations during SWNT growth. Both the structural unity and the high stability of Co nanoparticles suggest that they would serve as an ideal agent to grow SWNTs with a high chiral selectivity. While in a conventional CVD process with CO introduced into the reactor at ambient pressure, it was proven that SWNTs grown by a thermal decomposition of CO on Co nanoparticles (at 400°C, 500°C and 600°C, respectively) have narrow diameter distributions. Particularly, preferential growth of semiconducting SWNTs (~90%) with an exceptionally high population of (6, 5) tubes (53%) has been achieved at 500°C. In addition, we demonstrated a shift of the chiral preference from (6, 5) to other chiralities at a temperature as low as 400°C.

Results

Crystallography studies of the $Co_xMg_{1-x}O$ solid solution. The $Co_xMg_{1-x}O$ solid solution was prepared by impregnating porous MgO with a $Co(NO_3)_2$ aqueous solution, followed by high temperature calcination in air. In order to facilitate the later epitaxial formation of Co nanoparticles from the solid solution, the calcination process was optimally performed at 1000°C for 20 h. The resulting material was first characterized by X-ray diffraction (XRD). An XRD pattern (Fig. 1a) indicates that the crystal structure of the material remains in a single homogeneous phase which is isomorphic to that of a pure face-centered cubic (*fcc*) MgO (a = 0.422 nm) (Supplementary Fig. S1a). High-resolution TEM (HRTEM) imaging (Fig. 1b) of a representative cubic particle of the $Co_xMg_{1-x}O$ solid solution clearly exhibits uniform *fcc* (200) lattice fringes (Inset of Fig. 1b) of the well-defined single crystal structure. Energy-dispersive X-ray spectroscopy (EDX) analysis of the same $Co_xMg_{1-x}O$ particle demonstrates the coexistence of not only O and Mg but especially also Co in addition to spurious Cu signals that arise from the TEM grid (Fig. 1c). The above results prove the formation of a homogeneous $Co_xMg_{1-x}O$ solid solution.

***In situ* E-TEM observation of the $Co_xMg_{1-x}O$ catalytic dynamics and SWNT growth.** The above-prepared $Co_xMg_{1-x}O$ catalyst was heated in the specimen chamber of an E-TEM to 600°C. During the heating process, the specimen chamber was flushed with Ar at a pressure of 6.3 mbar. When the system became stable, a high-resolution scanning transmission electron microscope (STEM) dark-field image of a typical $Co_xMg_{1-x}O$ particle was acquired (Supplementary Fig. S1b) and it showed that the surface of the particle was very clean. No metal nanoparticles were observed. In contrast, when Ar was replaced with CO at the same pressure, nanoparticles with a monodisperse size distribution were observed on the MgO surface, which are clearly displayed as small bright dots in the STEM dark-filed images (Supplementary Fig. S1c). The dynamics of the nucleation of the nanoparticles and their temporal evolution under the CO reduction are revealed in Supplementary Movie S1, which was recorded in real time in the microscope operated in the bright-field imaging mode. In the movie, the dark-contrast nanoparticles are metal Co nanoparticles. With the introduction of CO, the Co cations in the $Co_xMg_{1-x}O$ catalysts were reduced in the solid phase, then quickly migrated to the surface and finally crystallized into metal nanoaprticles[36]. The Co^{2+} reduction is assumed to take place only in the top few atomic layers[33,37] while reduction of the underlying Co^{2+} is hampered due to their strong interaction with MgO in the solid solution[36]. By following the size evolution of six Co clusters in Supplementary Movie S1, one can see that all of them tend to form quickly stable nanoparticles with certain diameters (Supplementary Fig. S2a, S2b). A typical HRTEM bright-field image (Fig. 2a) shows the distribution of homogeneous Co nanoparticles on the surface of the MgO support. As measured from TEM images, Co nanoparticles feature

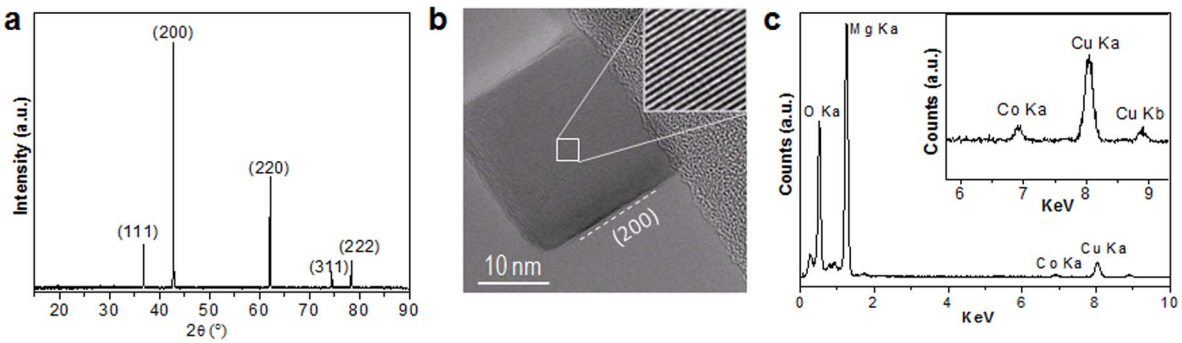

Figure 1 | Crystallography studies of as-prepared $Co_xMg_{1-x}O$. **a**, A XRD pattern of the $Co_xMg_{1-x}O$ solid solution. **b**, A TEM image of a representative cube particle of the $Co_xMg_{1-x}O$ solid solution with a close up of the particle as an inset showing clearly lattice fringes of the structure. **c**, An EDX spectrum of the materials measured on a similar particle to that shown in **b**. The region of interest (inset) indicates the presence of Co in the materials. The spurious Cu signals originate from the TEM grid.

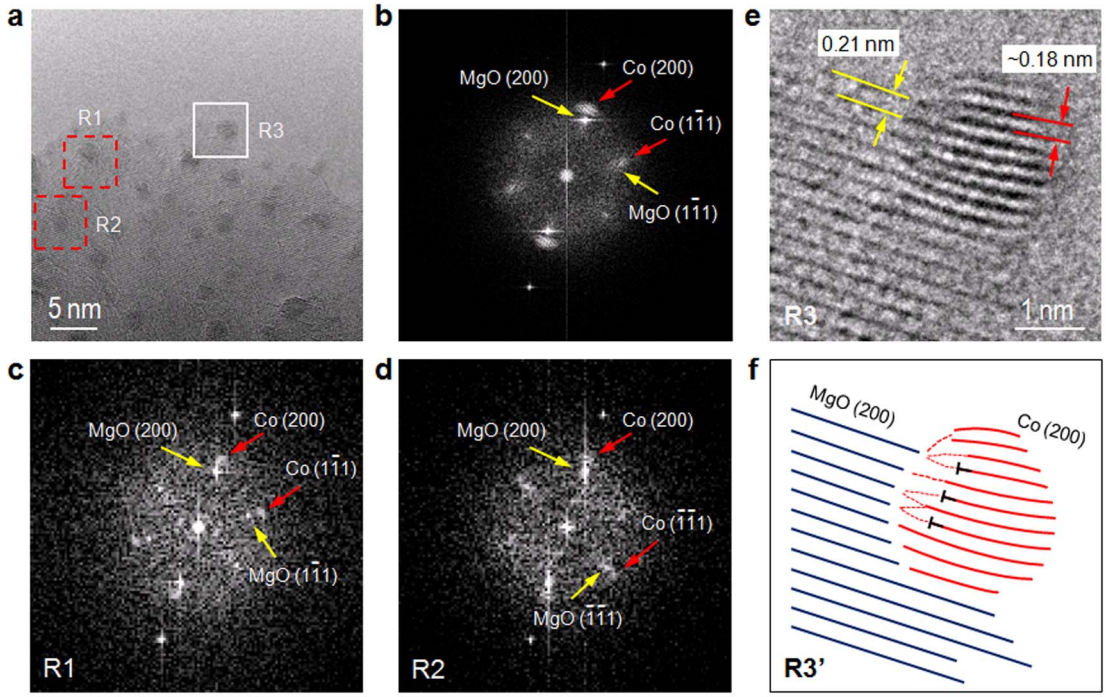

Figure 2 | *In situ* E-TEM studies of the epitaxially-formed Co nanoparticles. **a**, An *in situ* HRTEM lattice image of Co nanoparticles formed from the $Co_xMg_{1-x}O$ solid solution after introducing 6.3 mbar CO into the TEM chamber at 600°C. **b**, The FFT digital diffractogram calculated from the whole image of **a**, showing in general the epitaxial relationship between *fcc* Co nanoparticles and the *fcc* MgO matrix. **c** and **d**, FFTs of selected regions in **a** denoted by R1 and R2, respectively, show well-defined [011]-zone axis patterns for both *fcc* MgO and *fcc* Co. **e**, A close-up of the framed area R3 in **a** displays the atomic arrangement of the epitaxial structure. **f**, A schematic representation of the Co-MgO lattice configurations, showing the formation of interfacial misfit dislocations and the severe lattice deformations in the Co nanoparticle.

a narrow diameter distribution with a mean diameter of 1.8 nm (Supplementary Fig. S2c).

From the HRTEM image (Fig. 2a) the Fast Fourier transform (FFT) was calculated. The digital diffractogram (Fig. 2b) displays spots for both the MgO matrix and the Co nanoparticles. The spots in the FFT can be indexed to *fcc* MgO ($a = 0.422$ nm) and *fcc* Co ($a = 0.354$ nm) structures, respectively, both along [011] zone axes. Despite the fact that the spots for Co are either smeared (e.g. 200) or diffusely mixed with those for MgO (e.g. 1 1 1) due to, mainly, the averaging effect of the FFT over a large image area, we can conclude that all Co nanoparticles adopt a common crystallographic orientation [011] with little deviation. This is additionally confirmed by Fourier analysis of the two selected regions in Fig. 2a, denoted by R1 and R2, respectively. Both FFTs (Fig. 2c and 2d) show well-defined [011] patterns (indicated with arrows) for both *fcc* MgO and *fcc* Co, which demonstrates unambiguously an epitaxial relationship between Co nanoparticles and the MgO matrix, characterized by Co[011]//Mg[011] and Co(200)//MgO(200). A zoomed-in view (Fig. 2e) of the framed region R3 in Fig. 2a demonstrates the resulting epitaxial structure, and a schematic of such a lattice-mismatched epitaxy is shown in Fig. 2f. Due to an unusually large mismatch in the lattice constants between the two materials (~16%), the Co nanocrystal is severely strained to accommodate the lattice of the MgO matrix. Although misfit dislocations form at the interface to partially relax the strain, the residual misfit strain causes apparent deformation of the Co lattice, which preferably decreases the interface area, thus prevent forming large diameter Co nanoparticles[28]. Despite the observed lattice deformation and the interfacial misfit dislocations, the Co nanoparticle itself is defect free. In addition, the Fourier transform of the image in Fig. 2e indicates a slight misorientation (~5°) between Co and MgO (Supplementary Fig. S3),

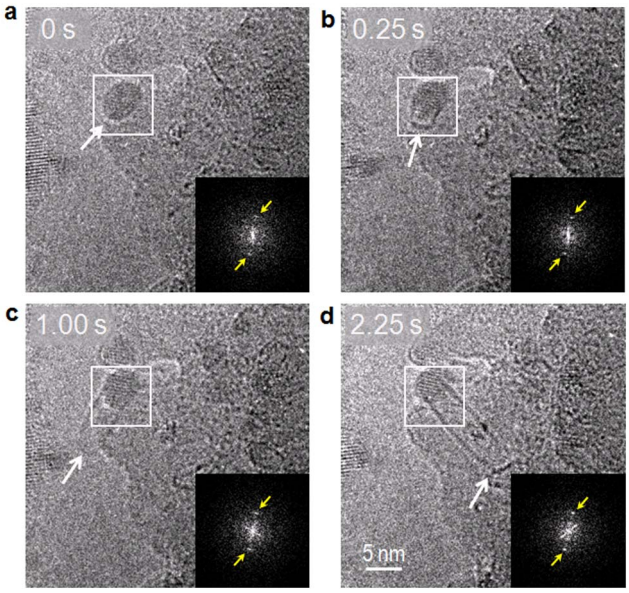

Figure 3 | *In situ* time-resolved E-TEM observations of SWNT growth. A time-sequence of four still E-TEM images (extracted from Supplementary Movie S2) of a Co-catalyzed SWNT grown at 600°C in presence of CO at 6.3 mbar. A time stamp accompanies each image. Insets: FFTs of the Co nanoparticle (framed) in each corresponding image, showing a negligible fluctuation in its crystal orientation during SWNT growth.

probably because of the uneven strains imposed on the Co at the edge of the matrix.

Such epitaxially formed Co nanoparticles usually exhibit homogeneous morphology and crystal structure[27–29], especially, high structure stability, by being anchored to the MgO support. Thus, they have the potential to catalyze the growth of SWNTs with structural uniformity. By further feeding CO into the E-TEM chamber, SWNTs were observed growing from catalytic Co nanoparticles. Atomic-resolution real time E-TEM movies showing the growth of SWNTs from Co nanoparticles are provided in Supplementary Movie S2 and S3. A time-sequence of four still images extracted from Movie S2, and six from Movie S3 are shown in Fig. 3 and Supplementary Fig. S4, respectively. The inset in each image shows the FFT of the framed region in the corresponding image. In contrast to similar E-TEM observation previously reported where the structures of those supported transition metal nanoparticles fluctuate remarkably during carbon nanotube growth[24,25], our observations here, as clearly indicated by the FFT analysis, demonstrate that the Co nanoparticle shows little fluctuations in its crystal orientations during SWNT growth (Fig. 3 and Supplementary Fig. S4), though the carbon nanotube grown on it swings from side to side (Supplementary Movie S2). This observation is in agreement with tight binding Monte Carlo (TBMC) simulations[38]. Here we note that only SWNTs with relatively large diameters were observed in the above-described *in situ* growth process. This is because of the extremely low pressure of CO allowed in the reaction chamber of the E-TEM. Such a low precursor pressure hampers the formation of small diameter nanotubes because small nanoparticles have a higher carbon solubility thus require a higher threshold precursor pressure for nanotube nucleation[39,40]. On the other hand, the microscope was operated at an accelerating voltage of 300 kV. The high-energy electrons may cause severe knock-on damage which destructs the carbon nanotube and induce structural defects[41,42]. Thus, carbon nanotubes shown in the movies appear defective, which was often observed in earlier similar E-TEM experiments[24,25]. Examples showing initial carbon cap formation on two Co nanoparticles, each around 1.8 nm in diameter, are provided in Fig. 4. Similar lattice-mismatched epitaxial relationship between Co and MgO, as demonstrated in Fig. 2e, was also observed in both cases.

Selective growth of SWNTs under ambient pressure of CO. As discussed above, due to the use of high-energy electrons and the low reaction pressure (6.3 mbar) of CO restricted in the E-TEM chamber, the produced SWNTs are usually defective and have large diameters. In order to make full use of the unique properties of the epitaxially-formed Co nanoparticles in structure-controlled growth of SWNTs, the $Co_xMg_{1-x}O$ solid solution was used as the catalyst to grow SWNTs in a CVD process with CO at ambient conditions. Similar to the *in situ* growth process, $Co_xMg_{1-x}O$ powders were loaded into a CVD reactor before they were heated up to a desired temperature in an Ar atmosphere. Later, a pure CO flow (50 cm^3/min) was introduced into the reactor to replace Ar as the carbon precursor for nanotube growth. The typical growth time was about 10 min. Fig. 5a shows a representative TEM image of SWNTs grown at 600°C on a typical cubic particle of the $Co_xMg_{1-x}O$ solid solution. A magnified image of the framed area in Fig. 5a is shown in Fig. 5b where a small diameter SWNT (0.74 nm) is displayed. More scanning electron microscopy (SEM) and TEM images are provided in the Supplementary Fig. S5 showing a general view of the purified carbon nanotubes. The carbon nanotubes are further characterized by optical measurements including Raman, absorption and photoluminescence (PL) spectroscopy. Fig. 5c shows the radial breathing mode (RBM) regions of three resonance Raman spectra which were taken at three different excitation wavelengths (514 nm, 568 nm, 647 nm), where only a small number of RBM peaks were observed in the range from 250 cm^{-1} to 350 cm^{-1}. This suggests that the investigated SWNTs have a narrow diameter distribution with a small mean diameter. Furthermore, the PL excitation/emission map (Fig. 5d) and the UV-vis-NIR absorption spectrum (Supplementary Fig. S6) from the sample demonstrated that the SWNTs grown on the $Co_xMg_{1-x}O$ solid solution at 600°C are composed of mainly (6, 5), (8, 3) and (7, 5) tubes with a high abundance of the semiconducting (6, 5) species.

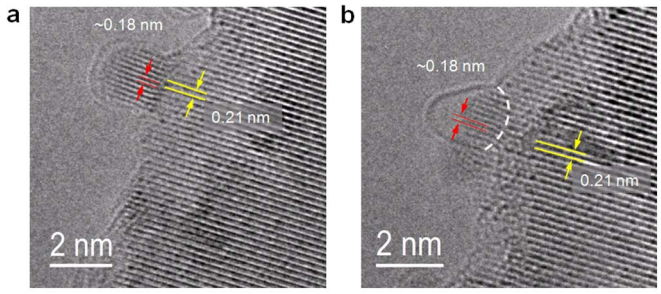

Figure 4 | Initial carbon cap formation on Co nanoparticles. **a**, **b**, *In situ* HRTEM lattice images showing carbon cap formation on epitaxial Co nanoparticles formed from the $Co_xMg_{1-x}O$ solid solution at 600°C in presence of 6.3 mbar CO in the TEM chamber. The lattice-mismatched epitaxial relationship between Co and MgO, as demonstrated in Fig. 2e, is also observed in both cases.

It was found that the growth temperature plays an important role in the preferential growth of SWNTs with a certain feature of chirality distribution. Compared with those grown at 600°C, SWNTs grown at 500°C show an exceptionally high concentration of the (6, 5) species, which was demonstrated by the PL measurement. Fig. 6a is a PL contour plot of the carbon nanotube sample grown at 500°C, where only one major peak corresponding to the (6, 5) tube was visible. The clear difference between Fig. 6a and Fig. 5d reflects the contrast of chirality and diameter distribution of SWNTs in the two samples that were grown at different temperatures. In order to further investigate the actual chirality components in the 500°C-grown sample with no constraint of the PL measurement to only semiconducting SWNTs[43,44], the electron diffraction (ED) technique[45] was employed which allows direct (*n, m*) measurements of individual SWNTs. Supplementary Figure S7 show TEM images of both as-grown SWNTs and dispersed SWNTs. By TEM statistic analysis, the SWNT purity is calculated to be about 85%. Electron diffraction patterns of three individual SWNTs are shown in Supplementary Figure S8, from which their chiral indices have been indexed as (6, 5) (Supplementary Fig. S8a), (7, 4) (Supplementary Fig. S8b) and (8, 3) (Supplementary Fig. S8c), respectively. A total number of 57 SWNTs have undergone electron diffraction analysis and the statistic results (Fig. 6b and Supplementary Table S1) reveal that only 11 chiral species were observed in the sample, of which about 53% (30 out of 57) are (6, 5) nanotubes. Additionally, the SWNTs have a very narrow diameter distribution (0.77 ± 0.05 nm), as indicated in Fig. 6c. In particular, nearly 90% of the investigated SWNTs are semiconducting. Interestingly, metallic armchair SWNTs, which are supposed to have high growth rate[46], however, were not observed in our experiment.

When further reducing the growth temperature down to 400°C, the chirality preference of the produced SWNTs shifts to (7, 6) and (9, 4) nanotubes, which is evidently displayed in their PL contour plot map shown in Supplementary Fig. S9. In contrast to the PL maps of the other two samples previously discussed, the PL map of the 400°C sample shows no evidence of (6, 5) tubes. The PL measurements indicated that the SWNTs grown at 400°C have a relatively large mean diameter (~0.90 nm). Therefore, we have demonstrated that SWNTs with a narrow chiral distribution can possibly be grown at a temperature as low as 400°C.

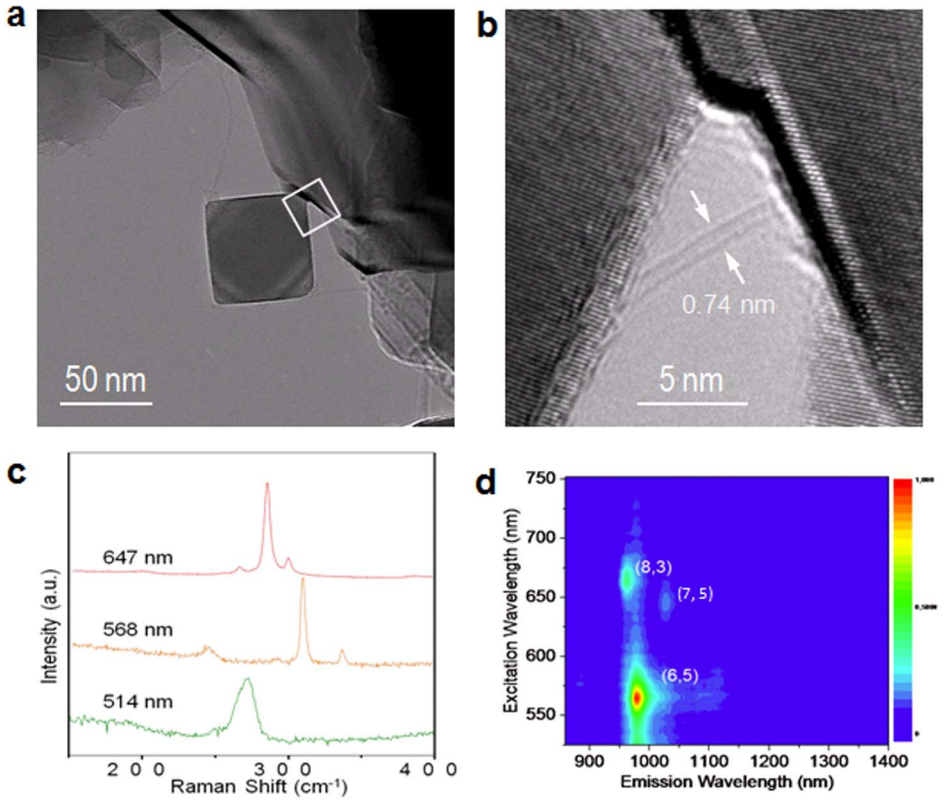

Figure 5 | ***Ex situ* characterizations of SWNTs.** **a**, An *ex situ* TEM image of SWNTs grown on the $Co_xMg_{1-x}O$ catalyst in a regular CVD process at 600°C with CO as carbon source under ambient pressure. **b**, A close-up of the previous image where an isolated SWNT with a small diameter is indicated by arrows. **c**, RBMs in Raman spectra (at three different excitation wavelengths) of SWNTs dispersed in a sodium cholate aqueous solution. **d**, Contour plots of the normalized PL emission intensities under various excitation energies for the SWNT sample.

Discussion

It is worth remarking that an enrichment in (6, 5) nanotubes has been widely reported in a number of catalyst systems, typically in bimetallic catalyst systems such as CoMo[9,21,40], CoMn[12], FeRu[10], NiFe[20] and FeCu[11]. Various growth strategies, like high pressure[12,40] and the use of Fe catalyst[10,11,20] have been attempted to achieve such a preference. The actual cause for high preference towards (6, 5) remains veiled in mystery and deserves further dedicated investigation. In this work, the way of forming uniform Co nanoparticles is unique and the (6, 5) selectivity has been largely improved at certain growth conditions compared to those previously reported results. In particular, we also demonstrated a shift of the chiral preference from (6, 5) to other chiralities by tuning the growth temperature. We believe that our unique preparation of epitaxial Co nanoparticles promote the high chiral selectivity. The strong Co-MgO epitaxial interactions played important roles in regulating the crystal structure of Co nanoparticles that serve as templates for initial carbon cap formation[18,20] as well as the subsequent thermodynamically favorable growth of SWNTs with a particular chiral structure[47]. As comparisons, SWNTs grown from similar catalytic systems which lack such an epitaxial relationship, e.g. monometallic Co catalyst on an oxidized Si wafer[16], SiO_2-supported Co catalyst[13], cobalt-incorporated MCM-41 (Co-MCM-41) catalyst[48] and SiO_2-supported CoMo catalyst[9], all display far broader chirality distributions.

Although the chiral majority shifts toward the small-diameter direction when the growth temperature decreases from 600°C to 500°C, it should be noted, however, that by further lowering the growth temperature down to 400°C, the chiral preference appears to be (7, 6) and (9, 4) nanotubes with slightly increasing diameters. This is in a good agreement with a recent study[39] which explicitly showed that, when the reaction temperature is lower than a threshold value, small catalyst particles are preferably deactivated for growing nanotubes due to an encapsulation by disordered carbonaceous envelopes, thus resulting in the lack of small diameter SWNTs at an extreme low temperature.

To summarize, by optimizing the preparation conditions of a $Co_xMg_{1-x}O$ solid solution catalyst we have succeeded in achieving an epitaxial formation of monometallic Co nanoparticles by reducing the solid solution in CO. Thus, for the first time, this type of catalyst was applied to grow SWNTs with the aim to enhance chiral selectivity. The dynamic behavior of the catalytic Co nanoparticles was studied using an environmental transmission emission microscope, inside which the nucleation and growth of SWNTs in the presence of CO at a low pressure was observed in real time. High-resolution TEM imaging analysis disclosed the *fcc* structure of the formed Co nanoparticles and revealed their epitaxial relationship with the MgO support. Especially, they exhibit a structural uniformity and have little fluctuations during SWNT growth due to a unique lattice-mismatched epitaxial interaction with the MgO matrix. The distinctive properties of epitaxial Co nanoparticles promoted highly chiral-selective growth of SWNTs in an ambient CO atmosphere at a range of temperatures. We showed that SWNTs can be grown from the thermal decomposition of CO on Co nanoparticles at 400°C, 500°C and 600°C, respectively, and they all feature narrow diameter distributions. In particular, we have achieved a preferential growth of small-diameter semiconducting SWNTs at 500°C. Moreover, we succeeded in growing chirality-selected SWNTs at a low reaction temperature (400°C), and demonstrated a shift of the chirality preference from (6, 5) tubes at 500°C to (7, 6) and (9, 4) nanotubes at 400°C. We attribute the high chiral selective growth to the structural similarity of monometallic Co nanoparticles formed through lattice-mismatched epitaxy in the $Co_xMg_{1-x}O$ solid solution.

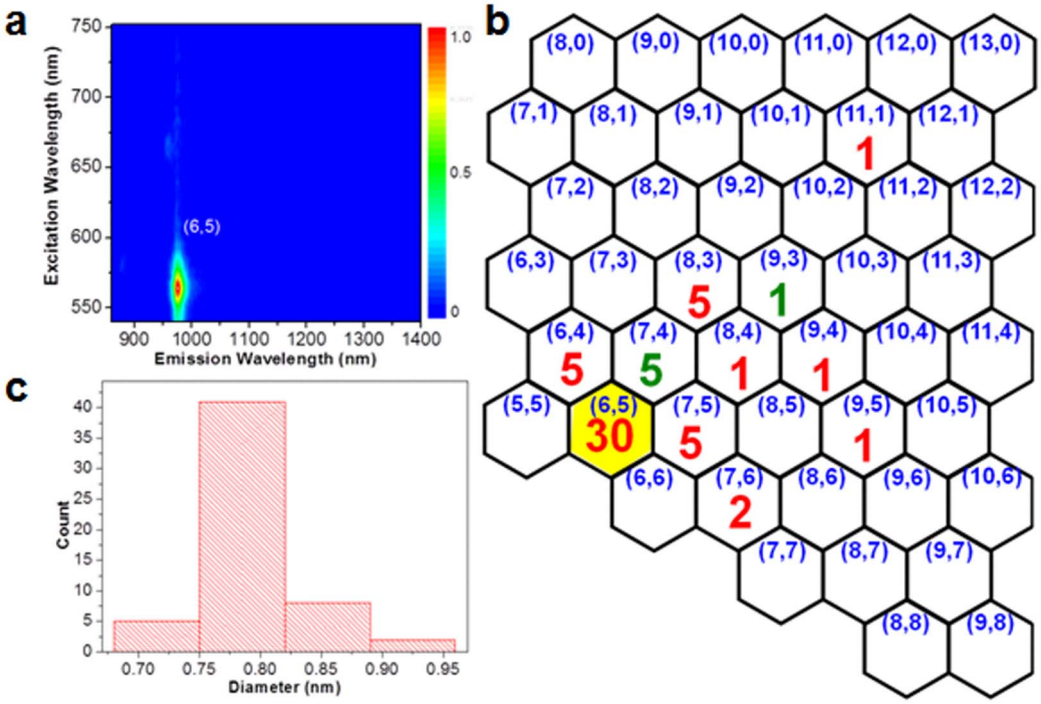

Figure 6 | A strong chiral preference demonstrated at a growth temperature of 500°C. a, A PL contour plot for the SWNTs grown on the $Co_xMg_{1-x}O$ catalyst in a CVD process under an ambient pressure of CO at 500°C, showing a high chiral selectivity of (6, 5) nanotubes. **b**, A chirality map of the same sample measured from ED analysis of totally 57 individual SWNTs. The occurrence of a nanotube with a certain chirality (*n, m*) is labeled in its corresponding hexagonal cell with red color for semiconducting tubes and green for metallic tubes. **c**, A histogram of diameter distribution of the produced SWNTs calculated on the basis of the ED analysis in **b**.

Methods

Sample preparations. The $Co_xMg_{1-x}O$ catalyst was prepared by an impregnation of porous MgO with a $Co(NO_3)_2$ aqueous solution followed by high temperature calcination. A porous MgO support was obtained by a thermal decomposition of magnesium carbonate hydroxide hydrate (99%, Sigma-Aldrich) at 400°C for 1 h[11]. 1.4 g of $Co(NO_3)_2$•$6H_2O$ (98%, Sigma-Aldrich) was first dissolved in 100 mL distilled water before being completely mixed with 4.0 g of the above-prepared MgO. Such mixture was dried in air overnight at 90°C, then calcinated at 1000°C for 20 h in a muffle furnace.

To catalyze SWNT growth, 20 mg of such prepared $Co_xMg_{1-x}O$ catalyst was placed in a cold-wall CVD micro-reactor (CCR1000, Linkam Scientific Instruments Ltd)[11,13] then heated up to a desired temperature (400°C~600°C) in an Ar atmosphere at a flow rate of 50 cm^3/min. CO (50 cm^3/min) was then introduced to replace Ar and used as the carbon source to grow CNTs. The growth time was set to 10 min. After that, the system was cooled down to room temperature under Ar atmosphere. All the above processes were maintained at an ambient pressure. The overall growth efficiency of the catalysts is evaluated by the carbon yield which is defined as the percent weight of carbon deposited per total catalyst weight[22]. The total carbon yield is 2.0% for 500°C and 2.8% for 600°C.

Catalyst characterizations. For structural characterization, the as-prepared catalyst was finely ground in ethanol using an agate mortar. A drop of the resulting suspension was cast onto a copper TEM grid covered with holey carbon film (400 mesh, Agar Scientific). The *ex situ* TEM imaging and EDX analysis were carried out using an aberration-corrected JEOL-2200FS FEG TEM/STEM operated at 200 kV. XRD measurements were performed with an X'pert Pro diffractometer (PANalytical B.V.) using Cu Kα radiation (λ = 0.1541 nm).

E-TEM studies. *In situ* E-TEM experiments were performed on an FEI Titan E-cell 80-300ST aberration-corrected (S)TEM operated at an accelerating voltage of 300 kV[49]. By virtue of the presence of specially-designed pumping system, the dedicated environmental TEM allows *in situ* catalysis experiments in gaseous environments up to pressures of 10 mbar and temperatures of 1000°C. Due to a spherical aberration corrector installed for the imaging lens (CEOS Germany), dynamic events at the atomic level can thus be recorded in real time. In our study, the finely ground catalyst particles were dispersed onto a bare Au grid (400 mesh, Agar Scientific), then loaded onto a tantalum double-tilt heating holder (up to 1000°C, Model 652, Gatan, Inc.), and later inserted into the TEM chamber. After that, the catalysts were heated up to 600°C in an Ar flow at a rate of 4.0 cm^3/min. When the pressure was stabilized at 6.3 mbar, the Ar was replaced with 5.0 cm^3/min CO to keep a constant pressure in the TEM chamber. High-resolution TEM imaging and high-angle annular dark-field STEM imaging were applied for *in situ* observation of the catalyst dynamics and the growth of SWNTs.

***Ex situ* characterizations of SWNTs.** The SWNTs grown in CO under an ambient pressure were characterized *ex situ* with both electron microscopy and optical measurements. For TEM imaging, the as-grown and purified carbon nanotubes were dispersed in acetone and a drop of such solution was spread onto a holey amorphous carbon film-coated Cu grid (400 mesh, Agar Scientific). SEM observations of the purified carbon nanotubes were carried out with a JSM-7500FA scanning electron microscope (JEOL Ltd.) operating at an acceleration voltage of 1 kV. For optical spectroscopic measurements, the produced SWNTs were first purified by hydrochloric acid (3.0 mol/L), then rinsed with H_2O and dried at 60°C overnight. The purified SWNTs were suspended in an aqueous solution of sodium cholate hydrate which was sonicated with a Branson DIGITAL Sonifier® (Models S-450D, PGC Scientific) for 1 h, followed by a high-speed centrifugation process at 50,000 g for another 1 h (Ultracentrifuge Optima Max-E, Beckman-Coulter, MLA-80 rotor). The resulting supernatant contained mostly isolated SWNTs, which was used for Raman (Jobin-Yvon S-3000 with Ar-Kr laser, Newport Stabilite-2018), UV-vis-NIR absorption (Perkin Elmer, Lambda 950), PL (Horiba Jobin-Yvon NanoLog-4) spectroscopy analysis, as well as for electron diffraction investigations.

For the electron diffraction experiment, a drop of the afore-prepared supernatant was spread onto a holey amorphous carbon film-coated Cu TEM grid. The grid was washed with formic acid, methanol and *iso*-propanol in sequence to remove possible remaining surfactants on the surface of carbon nanotubes, then annealed at 400°C in a high vacuum for 2 h. Electron diffraction experiments were carried out on a JEOL-2200FS FEG TEM/STEM operated at a low operating voltage of 80 kV, which is well below the electron knock-on damage threshold for carbon. The chirality determination of individual SWCNTs from their ED patterns was based on a calibration-free intrinsic layer-line spacing method[45].

1. Noorden, R. V. The trials of new carbon. *Nature* **469**, 14–16 (2011).
2. Hersam, M. C. Progress towards monodisperse single-walled carbon nanotubes. *Nature Nanotechnol.* **3**, 387–394 (2008).
3. Arnold, M. S., Green, A. A., Hulvat, J. F., Stupp, S. I. & Hersam, M. C. Sorting carbon nanotubes by electronic structure using density differentiation. *Nature Nanotechnol.* **1**, 60–65 (2006).
4. Ghosh, S., Bachilo, S. M. & Weisman, R. B. Advanced sorting of single-walled carbon nanotubes by nonlinear density-gradient ultracentrifugation. *Nature Nanotechnol.* **5**, 443–450 (2010).

5. Tu, X., Manohar, S., Jagota, A. & Zheng, M. DNA sequence motifs for structure-specific recognition and separation of carbon nanotubes. *Nature* **460**, 250–253 (2009).
6. Zheng, M. & Semke, E. D. Enrichment of single chirality carbon nanotubes. *J. Am. Chem. Soc.* **129**, 6084–6085 (2007).
7. Zheng, M. *et al.* DNA-assisted dispersion and separation of carbon nanotubes. *Nature Mater.* **2**, 338–342 (2003).
8. Liu, H., Nishide, D., Tanaka, T. & Kataura, H. Large-scale single-chirality separation of single-wall carbon nanotubes by simple gel chromatography. *Nat. Commun.* **2**, 309 (2011).
9. Bachilo, S. M. *et al.* Narrow (n,m)-distribution of single-walled carbon nanotubes grown using a solid supported catalyst. *J. Am. Chem. Soc.* **125**, 11186–11187 (2003).
10. Li, X. *et al.* Selective synthesis combined with chemical separation of single-walled carbon nanotubes for chirality selection. *J. Am. Chem. Soc.* **129**, 15770–15771 (2007).
11. He, M. *et al.* Predominant (6, 5) single-walled carbon nanotube growth on a copper-promoted iron catalyst. *J. Am. Chem. Soc.* **132**, 13994–13996 (2010).
12. Zoican Loebick, C. *et al.* Selective synthesis of subnanometer diameter semiconducting single-walled carbon nanotubes. *J. Am. Chem. Soc.* **132**, 11125–11131 (2010).
13. He, M. *et al.* Selective growth of SWNTs on partially reduced monometallic cobalt catalyst. *Chem. Commun.* **47**, 1219–1221 (2011).
14. Wang, H. *et al.* Selective synthesis of (9,8) single walled carbon nanotubes on cobalt incorporated TUD-1 catalysts. *J. Am. Chem. Soc.* **132**, 16747–16749 (2010).
15. Liu, B., Ren, W., Li, S., Liu, C. & Cheng, H. M. High temperature selective growth of single-walled carbon nanotubes with a narrow chirality distribution from a CoPt bimetallic catalyst. *Chem. Commun.* **48**, 2409–2411(2012).
16. Fouquet, M. *et al.* Highly chiral-selective growth of single-walled carbon nanotubes with a simple monometallic Co catalyst. *Phys. Rev. B* **85**, 235411 (2012).
17. Volotskova, O. *et al.* Tailored distribution of single-wall carbon nanotubes from arc plasma synthesis using magnetic fields. *ACS Nano* **4**, 5187–5192 (2010).
18. Reich, S., Li, L. & Robertson, J. Control the chirality of carbon nanotubes by epitaxial growth. *Chem. Phys. Lett.* **421**, 469–472 (2006).
19. Harutyunyan, A. R. *et al.* Preferential growth of single-walled carbon nanotubes with metallic conductivity. *Science* **326**, 116–120 (2009).
20. Chiang, W. H. & Mohan Sankaran, R. Linking catalyst composition to chirality distributions of as-grown single-walled carbon nanotubes by tuning NixFe1−x nanoparticles. *Nature Mater.* **8**, 882–886 (2009).
21. Resasco, D. E. *et al.* A scalable process for production of single-walled carbon nanotubes (SWNTs) by catalytic disproportionation of CO on a solid catalyst. *J. Nanopart. Res.* **4**, 131–136 (2002).
22. Alvarez, W. E., Kitiyanan, B., Borgna, A. & Resasco, D. E. Synergism of Co and Mo in the catalytic production of single-wall carbon nanotubes by decomposition of CO. *Carbon* **39**, 547–558 (2001).
23. He, M. *et al.* Growth mechanism of single-walled carbon nanotubes on iron–copper catalyst and chirality studies by electron diffraction. *Chem. Mater.* **24**, 1796–1801 (2012).
24. Hofmann, S. *et al.* In situ Observations of catalyst dynamics during surface-bound carbon nanotube nucleation. *Nano Lett.* **7**, 602–608 (2007).
25. Yoshida, H., Takeda, S., Uchiyama, T., Kohno, H. & Homma, Y. Atomic-scale in-situ observation of carbon nanotube growth from solid state iron carbide nanoparticles. *Nano Lett.* **8**, 2082–2086 (2008).
26. Gomez-Gualdron, D. A., McKenzie, G. D., Alvarado, J. F. & Balbuena, P. B. Dynamic evolution of supported metal nanocatalyst/carbon structure during single-walled carbon nanotube growth. *ACS Nano* **6**, 720–735 (2012).
27. Ferrando, R., Rossi, G., Nita, F., Barcaro, G. & Fortunelli, A. Interface-stabilized phases of metal-on-oxide nanodots. *ACS Nano* **2**, 1849–1856 (2008).
28. Henry, C. R. Morphology of supported nanoparticles. *Prog. Surf. Sci.* **80**, 92–116 (2005).
29. Silly, F. & Castell, M. R. Selecting the shape of supported metal nanocrystals: Pd huts, hexagons, or pyramids on SrTiO3(001). *Phys. Rev. Lett.* **94** (2005).
30. Hongo, H., Yudasaka, M., Ichihashi, T., Nihey, F. & Iijima, S. Chemical vapor deposition of single-wall carbon nanotubes on iron-film-coated sapphire substrates. *Chem. Phys. Lett.* **361**, 349–354 (2002).
31. Chen, P., Zhang, H. B., Lin, G. D., Hong, Q. & Tsai, K. R. Growth of carbon nanotubes by catalytic decomposition of CH_4 or CO on a Ni-MgO catalyst. *Carbon* **35**, 1495–1501 (1997).
32. Flahaut, E., Peigney, A., Laurent, C. & Rousset, A. Synthesis of single-walled carbon nanotube–Co–MgO composite powders and extraction of the nanotubes. *J. Mater. Chem.* **10**, 249–252 (2000).
33. Wang, H. Y. & Ruckenstein, E. Formation of filamentous carbon during methane decomposition over Co-MgO catalyst. *Carbon* **40**, 1911–1917 (2002).
34. Hu, Y. H. & Ruckenstein, E. Binary MgO-based solid solution catalysts for methane conversion to syngas. *Catal. Rev.* **44**, 423–453 (2002).
35. Cho, A. Y. & Arthur, J. R. Molecular beam epitaxy. *Prog. Solid State Chem.* **10**, 157–191 (1975).
36. Takehira, K. Highly dispersed and stable supported metal catalysts prepared by solid phase crystallization method. *Catal. Surv. Japan* **6**, 19–32 (2002).
37. Parmaliana, A. *et al.* Magnesia-supported nickel catalyst: II. surface properties and reactivity in methane ateam reforming. *J. Catal.* **141**, 34–47 (1993).
38. Fiawoo, M. F. C. *et al.* Evidence of correlation between catalyst particles and the single-wall carbon nanotube diameter: a first step towards chirality control. *Phys. Rev. Lett.* **108**,195503 (2012).
39. Picher, M., Anglaret, E., Arenal, R. & Jourdain, V. Processes controlling the diameter distribution of single-walled carbon nanotubes during catalytic chemical vapor deposition. *ACS Nano* **5**, 2118–2125 (2011).
40. Wang, B. *et al.* Pressure-induced single-walled carbon nanotube (n,m) selectivity on Co-Mo catalysts. *J. Phys. Chem. C* **111**, 14612–14616 (2007).
41. Krasheninnikov, A. V. & Banhart, F. Engineering of nanostructured carbon materials with electron or ion beams. *Nature Mater.* **6**, 723–733 (2007).
42. Banhart, F. Irradiation effects in carbon nanostructures. *Rep. Prog. Phys.* **62**, 1181–1221 (1999).
43. O'Connell, M. J. *et al.* Band gap fluorescence from individual single-walled carbon nanotubes. *Science* **297**, 593–596 (2002).
44. Bachilo, S. M. *et al.* Structure-assigned optical spectra of single-walled carbon nanotubes. *Science* **298**, 2361–2366 (2002).
45. Jiang, H., Nasibulin, A., Brown, D. & Kauppinen, E. Unambiguous atomic structural determination of single-walled carbon nanotubes by electron diffraction. *Carbon* **45**, 662–667 (2007).
46. Ding, F., Harutyunyan, A. R. & Yakobson, B. I. From the cover: dislocation theory of chirality-controlled nanotube growth. *Proc. Nat. Acad. Sci.* **106**, 2506–2509 (2009).
47. Yazyev, O. V. & Pasquarello, A. Effect of metal elements in catalytic growth of carbon nanotubes. *Phys. Rev. Lett.* **100**, 156102 (2008).
48. Chen, Y. *et al.* Low-defect, purified, narrowly (n,m)-dispersed single-walled carbon nanotubes grown from cobalt-incorporated MCM-41. *ACS Nano* **1**, 327–336 (2007).
49. Hansen, T. W., Wagner, J. B. & Dunin-Borkowski, R. E. Aberration corrected and monochromated environmental transmission electron microscopy: challenges and prospects for materials science. *Mater. Sci.Technol.* **26**, 1338–1344 (2010).

Acknowledgements

This work was funded by the CNB-E Project in Aalto University through the Multidisciplinary Institute of Digitalization and Energy (MIDE) program and the Aalto Energy Efficiency program project (MOPPI). M.H., H.J. and B.L. acknowledge financial support by the NorTEMnet project (NordForsk). F.C., T.W.H. and J.B.W. acknowledge supports from the A. P. Møller and Chastine Mc-Kinney Møller Foundation. P.V.F., A.I.C., E.A.O., A.V.B. and E.D.O. acknowledge financial supports in RFBR-10-02-00792, RFBR 12-02-31581 and MK-5618.2012,2 projects. The authors acknowledge the Laboratory of Inorganic Chemistry of Aalto-University for access to X-ray diffractometer and Mr. Matti Lehtimäki for his assistance with the measurements. This work made use of facilities from the Nanomicroscopy Center of Aalto University.

Author contributions

M.H. and H.J. designed and carried out the experiments. H.J. and M.H. conducted *ex situ* TEM observations and electron diffraction experiments with data analysis. M.H., H.J., B.L., F.C., T.W.H. and J.B.W. carried out *in situ* E-TEM experiments. P.V.F., A.I.C., E.A.O., A.V.B. and E.D.O. performed Raman spectroscopy, UV-vis-NIR absorption, PL measurements and data analysis. I.V.A. helped with TEM sample preparation of SWNTs for ED analysis. M.H. and H.J. co-wrote the manuscript. All authors discussed the results and commented on the manuscript.

Additional information

Supplementary information accompanies this paper at http://www.nature.com/scientificreports

Competing financial interests: The authors declare no competing financial interests.

How to cite this article: He, M.S. *et al.* Chiral-Selective Growth of Single-Walled Carbon Nanotubes on Lattice-Mismatched Epitaxial Cobalt Nanoparticles. *Sci. Rep.* **3**, 1460; DOI:10.1038/srep01460 (2013).